Influence of hemicellulose content and cellulose crystal change on cellulose nanofibers properties

Matheus Cordazzo Dias, Uasmim Lira Zidanes, Caio Cesar Nemer Martins, Ana Lázara Matos de Oliveira, Renato Augusto Pereira Damásio, Jaime Vilela de Resende, Eduardo Valério de Barros Vilas Boas, Mohamed Naceur Belgacem, Gustavo Henrique Denzin Tonoli, Saulo Rocha Ferreira

INFLUENCE OF HEMICELLULOSE CONTENT AND CELLULOSE CRYSTAL CHANGE ON CELLULOSE NANOFIBERS PROPERTIES

Matheus Cordazzo Dias[a,d*], Uasmim Lira Zidanes[a], Caio Cesar Nemer Martins[a], Ana Lázara Matos de Oliveira[b], Renato Augusto Pereira Damásio[c], Jaime Vilela de Resende[b], Eduardo Valério de Barros Vilas Boas[b], Mohamed Naceur Belgacem[d], Gustavo Henrique Denzin Tonoli[a], Saulo Rocha Ferreira[e]

***Corresponding author: Matheus Cordazzo Dias**, Department of Forest Science, Federal University of Lavras, C.P. 3037, 37200-900 Lavras, MG, Brazil, e-mail: matheus.cordasso@gmail.com https://orcid.org/0000-0002-8154-2543.

[a] Department of Forest Science, Federal University of Lavras, C.P. 3037, 37200-900 Lavras, MG, Brazil

[b] Department of Food Science, Federal University of Lavras, C.P. 3037, 37200-900 Lavras, MG, Brazil

[c] Klabin, Technology Center, Industrial R&D+I, Fazenda Monte Alegre, St. Harmonia, 84275-000 - Telêmaco Borba, PR, Brazil

[d] Université Grenoble Alpes, CNRS, Grenoble INP (Institute of Engineering Univ. Grenoble Alpes), LGP2, 38000, Grenoble, France

[e] Department of Engineering, Federal University of Lavras, C.P. 3037, 37200-900 Lavras, MG, Brazil

Abstract: This study aimed to evaluate the properties of cellulose nanofibers (CNFs) with different hemicellulose contents and cellulose II polymorphs. A link was found between these polysaccharides and the properties of CNFs. A decrease in crystallinity (from 69 to 63%) and changes in the crystalline structure of cellulose subjected to an alkaline environment were observed, promoting the partial conversion of cellulose I to cellulose II (from 2 to 42%) and preventing CNFs production at NaOH concentrations higher than 5%. Most treatments showed pseudoplastic fluid behavior, except for the 10% NaOH treatment over 2 hours, which showed Newtonian fluid behavior. The quality index of the reference CNFs (TEMPO-oxidized) was the highest (80 ± 3), followed by that of the 5% NaOH-treated (68 ± 3 and 22% energy savings compared to the untreated sample), and the untreated (63 ± 3) samples; and the 10% NaOH treatments had quality indices of 51 ± 3 and 32 ± 1, respectively.

Keywords: Cellulose nanofibers; Cellulose polymorphs; Nanocellulose; Polyose; Shear rheology.

1. Introduction

In recent years, there has been growing interest the production and application of cellulose nanofibers (CNFs). CNFs are usually obtained from fibers that have native cellulose polymorphs, known as cellulose I. There are three other types of cellulose polymorphs, cellulose II, III, and IV. Cellulose I and II are the most studied and most used in industrial applications. Some works in the literature report that the conversion of cellulose I to cellulose II hinders the nanofibrillation process [1,2].

Cellulose II can be obtained from native cellulose by mercerization and regeneration processes because it has a more stable structure. However, crystalline structure conversion through these processes results in materials with inferior mechanical properties [2].

One of the essential characteristics of nanocellulose-based materials is their complex rheology. Because of this characteristic, processing is challenging, especially finding the most suitable application according to its produced characteristics, which can vary [3] due to the source of the materials and the method by which the materials were obtained. The deformation of these suspensions at different shear rates is essential in various potential applications [3].

The rheology of an aqueous suspension of nanocellulose is influenced by hydrogen bonding between nanofibrils and water molecules [4], which is directly related to the efficiency and quality of nanofibrillation, where suspensions with high nanocellulose content have a gel-like appearance and consequently a higher viscosity. In comparison, less nanofibrillated materials have a more aqueous appearance and a lower viscosity. The viscosity of nanocellulose materials is an important factor that must be optimized to be low enough to enable the material's processing and high enough to improve the dispersion [5].

The morphological and chemical composition of the raw material affects the rheological and mechanical properties of the obtained cellulose nanomaterial and the quality of the final product [6–8]. The morphological properties of CNFs are dependent on the source and production process. However, CNFs has re-active surfaces, low densities (1.54 g/cm^3) when compared to other materials, and a high number of free hydroxyl groups that contribute to the grafting of various chemicals to reach specific properties [9].

Lignocellulosic biomass is formed by cellulose, hemicellulose, lignin, and other minor components that create a complex matrix structure with natural recalcitrance, resulting from both the intrinsic molecules' nature and their interactions [10]. These components do not occur individually in the cell wall structure but are linked together in the Lignin-Carbohydrate Complex through stable chemical bonds [11].

Hemicellulose is the second most abundant class of hydrophilic polysaccharides found in nature and in the plant cell wall, closely associated with cellulose and lignin in all higher

plants, where they represent 20 - 30% of the plant dry mass [12]. These polymers has much lower molar weight when compared to cellulose, and contains a considerable degree of ramifications between its chains, possessing a highly amorphous nature, unlike cellulose, and is more susceptible to chemical hydrolysis under milder conditions [13]. Hemicellulose has a large proportion of hydroxyl groups that are bound in intra- and intermolecular hydrogen bonds, making it more hygroscopic than cellulose, and some of these bonds naturally bind water to cellulose molecules [14].

Due the higher number of free hydroxyl groups, hemicellulose presents a highly hydrophilic nature, and together with its amorphous nature and ramified structure, causes it to swell greatly when in contact with water molecules [15]. The swelling of the hemicellulose also has a strong impact on the cellulose crystal structure, due to a strong bond with the cellulose surfaces [16]. These polysaccharides may have an important role to play in the production of CNFs, for example, Iwamoto et al. [17] demonstrated that hemicellulose acts as an inhibitor of the cellulose microfibrils coalescence, thus contributing to the ease of the nanofibrillation process.

The number of studies regarding CNFs production and applications has increased progressively; hence, it is essential to extend the knowledge of its behavior and the relations between its chemical composition and the performance of derived materials. Therefore, this study aimed to evaluate the effects of the modifications on the properties of eucalyptus CNFs, especially the rheology of those containing different hemicellulose levels and cellulose I/cellulose II polymorph ratios.

2. Experimental

2.1 Materials

Once-dried BHKP (Bleached eucalyptus kraft pulp) donated by Klabin S.A. (Paraná/Brazil), was used throughout this work. All the materials and chemicals were used as received from the manufacturers: deionized water; sodium hydroxide (NaOH) (ACS reagent, ≥98%, Sigma–Aldrich, Brazil); TEMPO (2,2,6,6-tetramethyl-1-piperidinyloxy free radical - $C_9H_{18}NO$) (ACS reagent, ≥98%, Alfa Aesar, Germany); hydrochloric acid (HCl) (ACS reagent,

37%, Neon, Brazil); sodium bromide (NaBr) (ACS reagent, 99%, Synth, Brazil); sodium hypochlorite (NaClO) (ACS reagent, ≥10%, Dinâmica, Brazil); absolute ethyl alcohol (C_2H_6O) (ACS reagent, 99%, Sigma–Aldrich, Brazil); 0.5 M cupriethylenediamine solution (ACS reagent, Dinâmica, Brazil) and sulfuric acid (H_2SO_4) (ACS reagent, 99%, Sigma–Aldrich, Brazil).

2.2 Alkaline treatment of cellulose kraft pulp

The alkaline treatment was performed under different concentration conditions and reaction times to achieve fibers with different hemicellulose contents. This step was carried out according to Dias et al. [18]. The pulp was treated with 5 and 10 wt% aqueous NaOH solution at 80 °C for 1 and 2 h under continuous stirring (800 rpm). After treatment, the fibers were filtered and repeatedly washed with deionized water until the pH reached neutrality. They were then dried in an air-circulating oven at 50 °C for 24 h.

2.3 TEMPO-mediated oxidation treatment of cellulose kraft pulp

This treatment was also performed as a quality reference to compare the CNFs properties obtained after the alkaline treatments. This step was based on the methodology of Fukuzumi et al. [19]. The fibers (1 g) were suspended in water (40 mL) containing TEMPO (0.016 g) and sodium bromide (0.1 g). The NaClO solution (10 mmol) was added to the slurry, and the mixture was stirred at room temperature for three hours, and a pH of 10 was maintained by adding drops of 0.5 M NaOH. Afterward, 100 mL of ethanol was added to quench the reaction, and the system pH was corrected to 7 by the addition of drops of 0.5 M hydrochloric acid (HCl).

2.4 Fourier Transformed Infrared Spectroscopy (FTIR)

To investigate the changes in functional groups of CNFs that the treatments may have caused, FTIR analyses were performed employing an Attenuated Total Reflectance (ATR) FTIR Spectrometer Varian 600-IR Series equipped with a GladiATR from Pike Technologies. The samples were scanned from 4000 to 600 cm^{-1} with 32 scans at a resolution of 4 cm^{-1}.

2.5 Monosaccharide's quantification

Monosaccharides (glucan, xylan, mannan and galactan) were determined after acid hydrolysis. The samples were hydrolyzed by adding 50 mg of fibers to 0.5 mL of 72 wt% sulfuric acid. The mixture was heated in a water bath at 30 °C for 1 h and then diluted to 4 wt% sulfuric acid concentrations with deionized water. The diluted mixture was then heated at 105 °C for 150 min before cooling on ice. An ion chromatography system (Dionex ICS 5000, USA) with a Dionex CarboPac PA1 column at 25 °C with a flow rate of 1 mL min^{-1} of MQ-water. The detector sensitivity was optimized by post column addition of 200 mM NaOH at a flow rate of 0.5 mL min-1 to perform the analysis.

2.6 Cellulose nanofibers (CNFs) production

Eucalyptus cellulose fibers were immersed in distilled water at 2 wt% consistency for three days to guarantee fiber swelling. Then, they were nanofibrillated by passing the pulp through an ultrafine grinder Supermasscolloider (model MKCA6-2, stone model MKGA6-80, Masuko Sangyo Co., Ltd., Japan). The stone speed was fixed at 1,500 rpm [18]. Five passes through the equipment were necessary to obtain cellulose nanofibers.

2.7 Turbidity, visual inspection, and stability of the suspensions

The turbidity, measured in Nephelometric Turbidity Units (NTU), of the CNFs suspensions was measured with a portable turbidimeter (Aqualytic, AL-250, wavelength 860 nm) on a CNFs suspension that was diluted to 0.1 wt% and stirred for 1 min with Ultra Turrax (IKA T-25) at 10,000 rpm. The suspensions were placed in the test locations for photo acquisition. Images were acquired at 0, 10, 30 min and 1, 2, 3, 4, 5, 6, 7, 8, and 24 h. Fiji software was used to estimate the CNFs decantation in the suspensions, and then stability was calculated according to Eq. 1 proposed by Silva et al. [20]:

$$\text{Stability} = \left(\frac{\text{Dispersed}}{\text{Total}} \right) \times 100\% \quad (1)$$

where "Dispersed" is the height corresponding to suspended particles, and "Total" is the height of all the liquid in the recipient location.

148 **2.7 Micro size area (µm²)**

149 The CNFs suspensions were characterized using a light microscope (Zeiss Axio AX10,
150 Germany). The suspensions were previously diluted to 0.1 wt%, stirred for 1 min with Ultra
151 Turrax (IKA T-25) at 10,000 rpm, and sonicated for five minutes in an ultrasonic bath to obtain
152 a better dispersion. Photographs were taken at 10x magnification and analyzed using Fiji
153 software. The microsized area was obtained by following the methodology described elsewhere
154 [21].

155 **2.8 Transmission Electron Microscopy (TEM)**

156 The morphology of the CNFs was investigated using a Tecnai G2-12 (FEI company,
157 USA) instrument with an accelerated voltage of 80 kV. Sample preparation and TEM
158 configurations followed recommendations described elsewhere [22]. Diameter measurements of
159 CNFs were performed for at least 300 individual structures per image using open-source
160 software biological image analysis Fiji [23].

161 **2.9 X-ray diffraction (XRD)**

162 XRD analyses were performed using a PANalytical X'Pert PRO MPD X-ray
163 diffractometer (Malvern Panalytical, UK) equipped with an X'celerator detector with a Cu-Kα
164 source (λ = 1.5406 Å) in the 2θ range of 10-40°, with a 0.066° interval at 4°/min step rate. The
165 equipment was operated at a tension of 45 kV and a current of 40 mA.

166 The theoretical coordinates of native cellulose Iβ (full width at half maximum (FWHM)
167 = 0.1) and cellulose II (FWHM = 0.1) were extracted from crystallography information data
168 (.cif) using the software Mercury 2020.2.0 (CCDC, UK) obtained from the Supplementary
169 Information accompanying the original work Nishiyama et al. [24].

170 The patterns were deconvoluted using the Gaussian function with Magic Plot 2.9
171 (Magicplot Systems, Russia). For the amorphous halo, the cellulose II pattern with full
172 width at half maximum (FWHM = 9), only varying its intensity, was used, as suggested
173 in the literature [25]. After deconvolution, the crystalline fraction (CF) was calculated from the

ratio between the area below all the crystalline peaks and the total area below the curve, determined after deconvolution from Eq. 2:

$$CF(\%)=\frac{\sum \text{Area}_{\text{Crystalline Peaks}}}{\sum \text{Area}_{\text{Crystalline Peaks}}+\text{Area}_{\text{Amorphous Halo}}} \times 100 \quad (2)$$

For each NaOH-treated sample, the cellulose I (CI) and cellulose II (CII) contents were determined. From the sum of the peak area of the same crystal system (∑area for cellulose I and ∑area for cellulose II), the CI and CII percentages were calculated using Eq. 3 and 4, which were proposed in a study by Oudiani et al. [26].

$$CI(\%)=\frac{\sum \text{Area}_{CI}}{\sum \text{Area}_{CI}+\text{Area}_{CII}} \times 100 \quad (3)$$

$$CII(\%)=\frac{\sum \text{Area}_{CII}}{\sum \text{Area}_{CI}+\text{Area}_{CII}} \times 100 \quad (4)$$

The crystallite size (CS) of the (200) plane peak was calculated according to Scherrer's equation (Eq. 5):

$$D=\frac{K \times \lambda}{\beta \times \cos\theta} \quad (5)$$

where D is crystallite size (Å), K (0.9) is a constant that refers to crystal shape, λ is the wavelength of the ray used (copper), β is the FWHM of the peak, in radians, and θ is Bragg's angle of (200) plane diffraction.

2.10 Rheological behavior

The rheological behavior of CNFs suspensions at a 1% wt concentration at 25 °C was studied on a HAAKE ReoStress 6000 (Thermo Scientific, Karlsruhe, Germany) rheometer coupled to a HAAKE A10 (Thermo Scientific) thermostatic bath and a universal temperature control system HAAKE UTM Controller (Thermo Scientific brand, Karlsruhe, Germany) using a CC25 DIN Ti concentric cylinder sensor (D = 25.0 mm; Gap = 5.3 mm). The Newton law (Eq. 6), Power-law (Eq. 7), and Herschel-Bulkley (Eq. 8) models were adjusted to the data of the second increasing curve to determine the fluid flow profile and obtain the viscosity. The adjustment of the models was performed by the Statistical Analysis System 9.1.2 statistical package (SAS Institute Inc, USA) using three repetitions:

$$\tau = \mu \times \gamma \quad (6)$$

where τ is the shear stress in (Pa), μ is the dynamic viscosity (Pa.s), and γ is the shear rate (s^{-1}).

$$\tau = K \times \dot{\gamma}^{n} \quad (7)$$

where τ is the shear stress in (Pa), K is the consistency index (Pa s^n), $\dot{\gamma}$ is the deformation rate (s^{-1}), and n is the flow behavior index (dimensionless).

$$\tau = \tau_0 + K \times \dot{\gamma}^{\eta} \quad (8)$$

where τ is the shear stress in (Pa), τ_0 is the yield stress in (Pa), K is the consistency index (Pa s^n), $\dot{\gamma}$ is the deformation rate (s^{-1}), and n is the flow behavior index (dimensionless).

The apparent viscosity values were evaluated at a shear rate of 100 s^{-1}, which, according to Souza et al. [27], corresponds to a deformation commonly suffered by fluids in industrial pipes due to processes such as pumping and agitation.

2.11 CNFs films casting

Films were formed by casting, in which 60 mL of samples (1 wt%) was sonicated (Sonifier model QR500, Ecosonics, Brazil) at 40% power of the ultrasound for homogenization and later poured onto 15 cm diameter acrylic Petri dishes. The samples were kept in an acclimatized room at 23 ± 2 °C and a relative humidity of 50% until water evaporation. CNFs films were formed after approximately seven days under those conditions.

2.12 Transparency at 550 nm (%)

The transmittance of the CNFs films was measured at a wavelength of 550 nm using a UV spectrophotometer (SP 2000 UV, Bel photonics, Italy) in photometric mode. For each sample, five measurements were performed for samples from at least three different films. The transparency (T_{550}) of the film samples was calculated according to Eq. adapted from the work of Sothornvit et al. [28]:

$$T_{550} = \frac{(\log \%T)}{b} \quad (9)$$

where %T is the percent transmittance and b are the film thickness (mm).

2.13 Mechanical properties of CNFs films

The tensile properties were measured with a tensile testing machine (Instron 3365, USA) equipped with a load cell of 5 kN capacity. The films with nominal dimensions of 100 mm x 15 mm were pulled at a speed of approximately 5 mm/min, starting with an initial separation of 50 mm between clamping jaws. The tensile properties of the samples were determined based on the ASTM Standard Method D 882–12. To measure the film thickness, a digital rapid advance micrometer (0–30 mm) with a resolution of 0.001 mm was used, and ten random measurements were made for each specimen. Six replicates of each film were tested.

2.14 Simplified quality index (*Q.I.)

Distinct CNFs were evaluated according to the simplified quality index (*Q.I.) adapted from the work of Desmaisons et al. [21]. In contrast with the original quality index, this adapted simplified version is based on four parameters (turbidity, transparency at 550 nm, Young's modulus, and area of microparticles), which are considered and used for the *Q.I. calculation according to the Eq. 10:

$$*\,\mathrm{Q.I.} = (3 \times \text{turbidity mark}) + (3 \times \text{transparency mark}) + (3 \times \text{Young's modulus mark}) + (1 \times \text{micro size mark}) \quad (10)$$

where the marks are calculated from the raw measured values as indicated in the original publication. The resulting Eq. 11 including the raw test values was therefore:

$$*\,\mathrm{Q.I.} = 0.3X_1 + 4.95\ln(X_2) - 0.108 \times X_3^2 + 3.81 \times X_3 - 2.67\ln(X_4) + 53.91 \quad (11)$$

where X_1 is the turbidity (NTU), X_2 is the transparency (%), X_3 is Young's modulus (GPa), and X_4 is the micro size area (µm²).

2.15 Statical analysis

Quantitative analyses that required repetition were submitted to statistical validation. Tukey's test at 95% significance was applied to investigate whether the averages were significantly different from those of the untreated sample. Statistical analyses were performed using the free software SISVAR version 5.6.

3. Results and discussion

To better communicate the results and facilitate the reading of the text, Table S1 summarizes each treatment carried out in this study, the materials, and their respective identification codes.

3.1 Hemicellulose quantification

Table 1 gives the chemical composition of the eucalyptus fibers before and after the TEMPO and alkaline treatments. All treatments involved removing the hemicellulose from the pulp, although the alkaline treatment was more efficient than the TEMPO treatment.

Table 1: Average and standard deviation of the cellulose and hemicellulose contents of Eucalyptus fibers (F) before and after TEMPO and alkaline treatments. * Different letters in the same column indicate significant ($\rho \leq 0.05$) differences between the samples for Tukey's test. ND = Not detected.

Samples	Cellulose (%)	Xylan (%)	Mannan (%)	Galactan (%)	Total hemicellulose (%)
Untreated_F	83.52 ± 0.44^{c}	16.14 ± 0.20^{a}	0.10 ± 0.14^{a}	0.04 ± 0.06^{a}	16.28 ± 0.40^{a}
TOF	84.83 ± 0.45^{c}	14.85 ± 0.01^{b}	0.22 ± 0.30^{a}	ND	15.17 ± 0.45^{b}
Na5_2_F	89.82 ± 0.77^{b}	9.84 ± 0.52^{c}	0.11 ± 0.16^{a}	0.03 ± 0.04^{a}	9.98 ± 0.72^{c}
Na10_1_F	95.77 ± 1.35^{a}	4.06 ± 0.26^{d}	ND	ND	4.06 ± 0.26^{d}
Na10_2_F	96.58 ± 1.13^{a}	3.30 ± 0.11^{e}	ND	ND	3.30 ± 0.11^{e}

The hemicellulose content decreased from 16.28 ± 0.39 in Untreated_F to 3.30 ± 0.11 in Na10_2_F. Higher NaOH concentrations and longer reaction times led to lower hemicellulose contents. Xylan was the major hemicellulosic compound in the fibers, despite treatment. Mannan and galactan were also found in the hemicellulosic fraction, but at extremely low proportions, lower than 0.22%. In fact, neither was detected in Na10_1_F and Na10_2_F, and galactan was not found in TOF. Hardwood pulp fibers such as those from Eucalyptus contain xylan, which is mainly located on the fiber surface, however, the mannan located between the dense structure of the elementary fibrils is difficult to contact directly in the alkaline solution [29]. The relative xylan content is higher than that in the corresponding inner layers after the kraft cooking process [30], where chemical attack is most efficient, which explains the effect of the treatments.

Hemicellulose presents a higher affinity for water than cellulose. Reducing the xylan content in the CNFs modifies the rheological behavior of the suspension, resulting in a weaker gel structure [31], which may affect the nanofibrillation efficiency.

3.2 Fourier Transform Infrared Spectroscopy (FTIR) analysis

The spectra of CNFs treatments ATR-FTIR analyses are shown in Figure 1. The band representing the O-H stretch band assignment differs between the treatments. In the NA 10_2_N and TONFC treatments peaks in this band occur. This indicates the presence of free hydroxyl (OH) in these samples.

[Figure 1 here]

Fig. 1. FTIR analysis of treatments and untreated CNFs.

The band at 2889 cm^{-1} present in the spectrum of TONFC, NA5_2_N, and NA10_2_N corresponds to the stretching vibration of CH [32,33]. Just the NA10_1_N treatment had the same behavior in this peak as the untreated one, so this treatment has no CH bonds in this band. Indicating the influence of the treatment on the nanofibrillation process.

The TEMPO-mediated oxidation treatment influences the chemical bonds of the CNFs the most, and it is possible to see the 1600 cm^{-1} peak present only in it. The absorption band due to C=O stretching of sodium carboxyl (CooNa) groups at 1600 cm^{-1}, was formed during the selective oxidation process of the C6 hydroxyl groups [34]. The treatment of CNFs with TEMPO-mediated oxidation differed in other results as well. The presence of this peak shows that the CNFs are indeed directly influenced by this treatment due to their chemical composition.

The peaks from 1154 to 897 cm^{-1} are characteristic when analyzing cellulose compounds [35–38]. The peak 1154 cm^{-1} is referring to C–O stretching. While the peak 1104 cm^{-1} represents the C–H bend. The chemical bond C–O stretching is represented at the peak of 1027 cm^{-1} of the graph. Both peaks 1027 cm^{-1} and 1154 cm^{-1} also represent the presence of xylan [39]. And the peak of 897 cm^{-1} corresponds to the C–H bend, which represents a type of cellulose I [39,40].

3.3 Turbidity, visual inspection, and stability of the CNFs suspensions

As expected, TOCNF showed the lowest turbidity (83 ± 5 NTU). The Na5_2_N treatment promoted less turbidity (359 ± 4 NTU) than the Untreated_N treatment (377 ± 3 NTU), suggesting that treatment with a solution of 5% NaOH can increase the degree of nanofibrillation of the material, while Na10_1_N and Na10_2_N showed the highest values (706 ± 8 and 912 ± 1 NTU, respectively), indicating less nanofibrillation and aggregation of these CNFs. The turbidity is linked to the material's size; if the suspension is only composed of nanoscale materials, the turbidity value is close to zero. However, the presence of non-nanofibrillated material in the suspension tends to increase the turbidity. These results demonstrate the importance of maintaining certain hemicellulose levels to avoid coalescence between the cellulose micro/nanofibrils.

The sedimentation analysis and the percentage stability over time allowed evaluation of the general stability of the aqueous CNFs suspensions (Fig. 2).

[Figure 2 here]

Fig. 2. A) Dispersion states of the 0.1 wt.% CNFs suspensions at 0, 10, 30 min, 1, 2, 3, 4, 5, 6, 7, 8, and 24 h. Influence of time on CNFs suspension stability in water.

TOCNF showed the most stable behavior (97% after 24 h compared to 74% Untreated_N) among all the samples, corroborating the previous results. Nanoscale cellulose particles are stable due to Brownian motion, which maintains the suspended particles through the interaction of repelling forces, according to Silva et al. [41].

The sedimentation results show a tendency of NaOH to strongly affect the stability of the suspension. After 24 h, the CNFs Na5_2_N showed a stability of approximately 62%, followed by Na10_1_N and Na10_2_N with 38% and 22% stability, respectively. The stability decrease may be related to two factors: (i) the removal of hemicellulose with the increase in alkali concentration and (ii) partial conversion of cellulose I to cellulose II. Hemicellulose acts as an inhibitor of cellulose coalescence. Therefore, as the removal of hemicellulose increases, the cellulose fibrils tend to agglomerate more, consequently decreasing the suspension stability.

During alkali treatment, cellulose microfibrils agglomerate via interdigitation. According to Lee et al. [42], the polarities of the cellulose II nanofibrils are the opposites of those of the adjacent nanofibrils; thus, neighboring nanofibrils intermingle into irregular aggregates.

3.4 CNFs morphology

Fig. 3 shows the CNFs networks of Untreated_N (Fig. 3a), TOCNF (Fig. 3b), Na5_2_N (Fig. 3c), Na10_1_N (Fig. 3d) and Na10_2_N (Fig. 3e).

[Figure 3 here]

Fig. 3. Typical transmission electron microscopy (TEM) and diameter distribution of CNFs and images from (A and F) Untreated_N; (B and G) TOCNF; (C and H) Na5_2_N; (D and H) Na10_1_N; and (E and J) Na10_2_N. The green arrows indicate more individualized CNFs, while purple arrows indicate more electrodense regions and consequently less individualized CNFs.

Note that as expected, TOCNF produced more individualized CNFs (indicated by green arrows) with smaller diameters (26 ± 20 nm), followed by Na5_2_N with an average diameter of approximately 34 ± 22 nm, while Untreated_N led to CNFs with an average diameter of approximately 45 ± 23 nm. Na10_1_N showed nanofibril structures with an average diameter of 77 ± 48 nm, and Na10_2_N showed structures with an average diameter greater than 100 nm (approximately 194 ± 171 nm). Taking into consideration the relationship between hemicellulose content and diameter of CNFs subjected to alkaline treatment, the results of this study showed similar trends with the results of the Lu et al. [39] study, where hemicellulose levels near 10% generated the smallest average diameters. These results are associated with the results obtained in the turbidity analysis, in which the treatments with smaller diameters were also those with lower turbidity values (Table 2).

With the excessive decrease in the hemicellulose content before the CNFs is obtained (Figs. 3d and 3e), the products have larger diameters, indicating less fibril individualization, evidencing, once again, the role of these noncellulosic polysaccharides as regulators of the morphological properties of the CNFs.

More intense alkaline treatments led to a higher degradation of hemicellulose (xylan) from the fiber structure, forming aggregates of cellulose fibrils and affecting the CNFs network

structure (Figs. 3d and 3e). Furthermore, surface xylan played a significant role as an electrostatic stabilizer in the CNFs dispersions by reducing the cohesion energy between the fibrils, whereas the removal of xylan drastically changed the CNFs dispersion properties [43,44].

Fig. 3 also shows the diameter distribution of CNFs produced under different conditions. With average diameters lower than 30 nm, which make the CNFs potentially useful as reinforcing agents in composites [45], the content of CNFs was approximately 33%, 72%, and 62% for Untreated_N, TOCNF, and Na5_2_N, respectively, and approximately 12% and 0% for Na10_1_N and Na10_2_N, respectively. These results indicate that the alkali-treated sample containing approximately 10% hemicellulose (Na5_2) was the only one that led to better nanofibrillation and individualization of the fibrils. This treatment presented more homogeneous nanofibrils, with 62% of the elements measured within the class of diameter of 15-30 nm, surpassing even the TOCNF treatment that presented 41% of the elements measured within the same class. Dias et al. [18] stated that hemicellulose content in the range of approximately 9 to 12% facilitates cell wall deconstruction.

TOCNF showed a slight reduction in hemicellulose content (from ~16% to ~15%), and it was the treatment with the best level of nanofibrillation. However, it is essential to note that, unlike other treatments, TEMPO-mediated oxidation promotes cellulose chemical modification through the selective oxidation of C6 hydroxyl groups by inserting carboxyl and aldehyde groups [19].

The darker regions in Figs 2d and 2e overlap, showing less individualization in these samples. The darker color (purple arrows) indicates a more electrodense region. The beam electrons cannot be transmitted in these regions, meaning that they are thicker than in Figs. 3a, 3b, and 3c.

Figs. 3a (Untreated_N), 3b (TOCNF), and 3c (Na5_2_N) more prominently show that these samples had better-structured CNFs networks (mainly in Figs. 3b and 3c) compared to the others. The more efficient the fibrils' individualization was, the greater the surface area of the material, allowing it to have more sites available to bind with water molecules improving the

CNFs network's swelling, contributing to its final gel consistency. According to Pääkkönen et al. [31], the swelling level has a considerable contribution to the gel network's quality, rheological behavior, and dewatering behavior of CNFs suspensions.

3.5 X-ray diffraction (XRD)

Fig. 4 shows that samples Untreated_N and TOCNF present the typical parallel crystalline structure of cellulose Iβ with peaks at 2θ = 14.9°, 16.4°, 20.5°, 22.6 and 34.7°, corresponding to lattice planes (1-10), (110), (102), (200) and (004), respectively [46]. Sample Na5_2_N presents all the mentioned peaks related to cellulose Iβ. However, a displacement of the peak at 2θ = 22.6° can be attributed to the beginning of the formation of an additional peak at 2θ = 22°. It corresponds to the lattice plane (020) of cellulose II, which may indicate the beginning of cellulose mercerization [26].

[Figure 4 here]

Fig. 4. Typical X-ray patterns of Eucalyptus CNFs samples obtained from fiber pulps before and after TEMPO and alkaline treatments. Characteristic peaks and the associated lattice planes are indicated for Cellulose Iβ (black dashed lines) and Cellulose II (red dashed lines), respectively. An amorphous halo of cellulose II with an FWHM of 9 is used as a reference for crystalline fraction calculation.

Fig. 4 also shows the partial conversion from native cellulose Iβ to cellulose II on fibers treated with an alkali concentration of 10% (Na10_1_N and Na10_2_N). The diffraction peaks observed at 2θ = 12.2°, 20.1° and 22.1° correspond to the (1-1 0), (110) and (020) lattice planes of cellulose II, respectively [46].

The crystalline fractions (CFs) were calculated using peak deconvolution and an area-based method because the amorphous component used in the Segal method is substantially influenced by the overlap of crystalline peaks [25]. Table 2 shows the modifications that occurred in the samples after the respective treatments. A higher CF average was found in Untreated_N, followed by TOCNF and the alkaline treatments Na5_2_N, Na10_1_N and Na10_2_N.

Table 2: Average and standard deviation values of the crystalline fraction (CF) and crystallite size (CS) for Eucalyptus CNFs produced under different conditions. Different letters in the same column indicate significant ($\rho \leq 0.05$) differences between the samples for Tukey's test.

Samples	Crystalline fraction (CF%)	Cellulose I (%)	Cellulose II (%)	Crystallite size (CS nm)
Untreated_N	69 ± 1^{a}	100	0	3.23 ± 0.02^{c}
TOCNF	67 ± 1^{a}	100	0	3.63 ± 0.03^{a}
Na5_2_N	67 ± 1^{a}	98	2	3.49 ± 0.04^{b}
Na10_1_N	63 ± 2^{b}	73	23	2.78 ± 0.01^{d}
Na10_2_N	63 ± 1^{b}	58	42	2.31 ± 0.01^{e}

All the treatments impacted the crystallinity of the cellulose. TEMPO-mediated oxidation preserved the native cellulose I structure of the sample. A slight (nonsignificant) decrease in TOCNF crystallinity was observed. This decrease in crystallinity may indicate that decrystallization of crystalline cellulose presumably occurred to some extent under oxidation [47].

The NaOH concentration also influenced the CF of the samples. As the NaOH concentration increased, CF decreased, probably due to the beginning of cellulose mercerization, inducing irreversible transformation of the native crystalline structure into cellulose II. According to Banvillet et al. [48], the formation of the cellulose II crystalline structure was globally less organized, leading to a decrease in crystallinity.

In Na10_1_N and Na10_2_N, cellulose II formation with antiparallel chains (Fig. 4) resulted in a gradual decrease in the cellulose I crystalline regions to soda cellulose I crystallites (Table 3). Cellulose I with antiparallel chains could absorb more alkaline solution, and then it was converted into cellulose II [26]. Furthermore, the conversion to cellulose II by the alkaline solution made fibrillation more complicated because of the aggregation via the interdigitation of micro/nanofibrils in the fiber's secondary cell wall [1].

The untreated sample had a crystallite size of 3.23 ± 0.05 nm (Table 3). The following TEMPO treatment led to an increase in CS (3.63 ± 0.03 nm). The explanation for this increase is that during TEMPO-mediated oxidation, the intra- and intermolecular repulsion increases with the selective oxidation of hydroxyl groups at C6, leading to an increase in crystallite size.

TEMPO-mediated oxidation is known to insert negative charges to form strong electrostatic repulsion between cellulose chains in water [49].

Na5_2_N also led to an increase in the CS (3.49 ± 0.04 nm). This increase may be due to the rearrangement in the crystal orientation and formation of some interstitial coalescence during the conversion of the (200) plane to the (020) plane [50]. In contrast, Na10_1_N and Na10_2_N showed decreased CS, 2.78 ± 0.01 nm, and 2.31 ± 0.01 nm, respectively. The stronger alkali solution could penetrate the crystalline regions, resulting in a disorder in the fiber crystallites, leading to decreased sizes [26].

3.6 Rheological behavior

The rheological behavior of the Eucalyptus CNFs suspensions was investigated at 25 °C. The curves of apparent viscosity as a function of shear rate are shown in Fig. 5.

[Figure 5 here]

Fig. 5. Apparent viscosity vs. shear rate for the CNFs suspensions under different conditions.

In Table 3, Newton's Law was adequately adjusted for Na10_2_N ($R^2 \geq 0.9544$), while the Power law and Herschel-Bulkley models were adjusted for Untreated ($R^2 \geq 0.9963$ and 0.9984, respectively), TOCNF ($R^2 \geq 0.9975$ and 0.9983, respectively), Na5_2_N ($R^2 \geq 0.9941$ and 0.9957, respectively) and Na10_1_N ($R^2 \geq 0.9883$ and 0.9963, respectively). All the samples presented low square root mean square error (RMSE) values (≤ 0.17).

Table 3: Parameters of the Newton model for EUC10% 2H and power law and Herschel-Bulkley models for Untreated_N, TOCNF_N, Na5_2_N, and N10_1_N.

Newton's Law						
Sample	**μ**	**Pr > t**	**R^2**	**RMSE**	**$\eta_{initial}$ (mPa.s)**	**η_{100} (mPa.s)**
Na10_2_N	0.0024	<.0001	0.9544	0.05	6.0 ± 2	2.0 ± 0.1

Power law							
Sample	**k ($Pa.s^n$)**	**n (-)**	**Pr > t**	**R^2**	**RMSE**	**$\eta_{initial}$ (mPa.s)**	**η_{100} (mPa.s)**
Untreated_N	2.08	0.34	<.0001	0.9963	0.17	1265 ± 26	99.0 ± 1.0
TOCNF_N	11.65	0.26	<.0001	0.9975	0.11	4450 ± 131	307.0 ± 5.0
Na5_2_N	1.01	0.34	<.0001	0.9941	0.10	635 ± 34	48.0 ± 0.7
Na10_1_N	0.08	0.52	<.0001	0.9883	0.04	70 ± 4	8.0 ± 0.1

Herschel-Bulkley

Sample	t	k (Pa.s^n)	n (-)	Pr > t	R^2	RMSE	$\eta_{initial}$ (mPa.s)	η_{100} (mPa.s)
Untreated_N	1.95	1.10	0.43	<.0001	0.9984	0.11	1265 ± 26	99.0 ± 1.0
TOCNF_N	3.89	9.10	0.29	<.0001	0.9983	0.10	4450 ± 131	307.0 ± 5.0
Na5_2_N	0.81	0.59	0.41	<.0001	0.9957	0.09	635 ± 34	48.0 ± 0.7
Na10_1_N	0.24	0.02	0.73	<.0001	0.9963	0.02	70 ± 4	8.0 ± 0.1

It was observed that the consistency index (K) was higher for TOCNF. A higher value of the (K) factor may indicate suspensions containing CNFs with a higher aspect ratio, which is expected for TEMPO-oxidized CNFs. The (K) and apparent viscosity seem to be strongly influenced by the hemicellulose content. It can be observed that the value decreases clearly from Untreated_N to Na5_2_N and almost reaches zero to Na10_1_N. According to Pääkkönen et al. [31], hemicellulose (especially xylan) is responsible for linking a significant amount of water to the fiber/CNFs structure, conferring higher viscosity to the suspensions, thereby increasing the (K) value.

The morphology of the material (each fibril) may be related to the (K) value. Poor nanofibrillated material (Na10_1_N and Na10_2_N) containing particles with larger dimensions leads to a weak fiber network with lower stiffness, facilitating its breaking and ordering when subjected to shear, thereby decreasing the viscosity [27].

Untreated_N presented flow index values of 0.34 (Power law) and 0.43 (Herschel-Bukley), while TOCNF presented the lowest values (0.26 and 0.29 for Power Law and Herschel-Bulkley, respectively). Na5_2_N presented flow index values of 0.34 and 0.41 (Power Law and Herschel-Bulkley, respectively), and Na10_1_N presented (n) values of 0.52 and 0.73 (Power Law and Herschel-Bulkley, respectively).

The flow index (n) depends on the structural properties of the entire suspension [51] and indicates the degree of non-Newtonian characteristics of the material. The values for all CNFs samples (except Na10_2_N) in the Power law and Hershel-Bulkley models point to pseudoplastic fluid behavior, presenting values lower than 1. Similar behavior was reported by Naderi et al. [52] when investigating the viscosity of softwood pulp and reported by Souza et al. [27] when studying the rheological behavior of Pinus, Eucalyptus, and cocoa shell CNFs. The decrease in viscosity is characteristic of pseudoplastic fluids as the shear rate applied to the fluid

489 increases (Fig. 5). This phenomenon is due to the state of order of the material present in the
490 stable solution, which is disordered, and, as shear is applied, it starts to become organized,
491 decreasing the viscosity.

492 The (K) values can also be linked as an indicator of the viscosity of the suspension,
493 while the (n) values can be related to the shear-thinning behavior of the suspension. Thus,
494 highly viscous suspensions would yield larger (K) values, while (n) values would decrease as
495 the suspensions become more thinning [53].

496 The rheology of nanocellulose suspensions is dependent on the structure, degree of
497 dispersion, degree of nanofibrillation, and interactions between the nanocellulose and the
498 solvent or matrix material [54]. The presence of a significant amount of surface hydroxyl groups
499 makes them easily dispersed in water and provides fluids with shear-thinning rheology and
500 thixotropy, even at low concentrations [55]. Rheological behavior characterization is essential
501 for understanding nanocellulose applicability to the use of nanocellulose-containing products
502 and processing issues related to coating, extrusion, molding, etc. [6].

503 Na10_2_N presented almost Newtonian flow, and the difference from the other
504 treatments may be due to the low efficiency of nanofibrillation. Fig. 3 shows that there was no
505 good deconstruction of the fiber cell wall in Na10_2_N, so there was no efficient
506 individualization of nanoscale fibrils, leading to the absence of a gel-like aspect. Geng et al. [56]
507 found that without reaching the gel-like point, the behavior of CNFs suspensions is almost
508 Newtonian.

509 The majoritarian presence of large particles may have contributed to this behavior, as
510 observed by Marchessault et al. [57], who studied the viscosity of cellulose microcrystal
511 suspensions and found that particle size influenced the rheological behavior of suspensions,
512 showing Newtonian behavior. The low concentration (1%) of this suspension (Na10_2_N) also
513 contributed to this behavior.

514 Due to its gel-like behavior, CNFs can be applied in the paper industry as a coating
515 layer on paper and paperboards. Coating processes such as bars and extrusion have the

advantages of high flexibility, absence of adhesive, and low production cost compared to a laminated system [58].

The rheological behavior of the CNFs may be correlated to the efficiency of nanofibrillation and the morphology of the material, which explains the lower viscosity of the CNFs of Na10_2_N; they have more non-nanofibrillated fibers than other CNFs. This discrepancy may result in the lack of a web-like network, which could facilitate breaking and ordering when the CNFs are exposed to shear force [27]. When nanofibrillation is effective, the surface area increases, and therefore, more interactions between fibril aggregates occur, leading to higher flow resistance of the suspension [59,60].

Two different types of behaviors can be observed in cellulose fiber suspensions: at lower shear rates, the pulp suspension is a Newtonian fluid, and at higher shear rates, pulp behavior is a non-Newtonian fluid [61].

Fig. 6 shows the apparent viscosity of CNFs at 100 s^{-1} under different conditions as a function of hemicellulose content. When the hemicellulose content in the CNFs increased, the apparent viscosity also increased, demonstrating a direct correlation (R^2 = 0.9966) between these two parameters. The hemicellulose content of Na5_2_N decreased by approximately 39% compared with that of Untreated_N, and the apparent viscosity decreased by approximately 52% at a shear rate of 100 s^{-1}. The hemicellulose content of Na10_1_N and Na10_2_N decreased by 75% and 80%, respectively, whereas the apparent viscosity at shear rate at 100 s^{-1} decreased 92% and 98%, respectively.

[Figure 6 here]

Fig. 6. The relationship between apparent viscosity and hemicellulose contents in the different CNFs after nanofibrillation. * EUC TEMPO was not considered in the correlation because, unlike the other fibers, it was a chemically modified fiber. Schematic representation showing how hemicellulose influences the separation of cellulose microfibrils. A) Representation of cellulose nanofibrils composed of crystalline and amorphous domains, both formed by ordered and disordered regions of cellulose chains; B) fibers with higher hemicellulose content being cut during nanofibrillation and being easily individualized; and C) nanofibrils from fibers with a low hemicellulose content are more difficult to individualize due to the coalescence between microfibrils.

However, in TOCNF, substitution by aldehyde and carboxyl groups in C6 caused the nanofibrils to create strong electrostatic repulsions with each other, allowing a greater number

548 of bonds with water molecules. This bonding resulted in a significant increase in the viscosity of
549 the suspension (210%), despite the slight loss of hemicellulose (~7%) due to oxidation in an
550 alkaline environment.

551 Hemicellulose plays an essential role in the nanofibrillation of wood pulp because its
552 presence impedes microfibril coalescence due to its ability to bind directly to cellulose
553 microfibrils through hydrogen bonds [62]. These results indicate that a higher hemicellulose
554 content supports CNFs individualization (as shown in Fig. 6) because of the increase in
555 viscosity, implying the formation of a complex network of CNFs. In contrast to cellulose, which
556 is more rigid than the other cell wall components, the behavior of hemicellulose is more plastic,
557 and hemicellulose can be plasticized, reducing the cohesion forces between the microfibrils
558 [63].

559 The viscosity of polymers and their solutions and suspensions is an essential transport
560 property that involves their process and applications. The rheological behavior of Untreated_N,
561 TOCNF, and Na5_2_N suspensions indicates that these can be applied in processes where
562 viscosity is a determinant, such as coating on the paper surface.

563 During the coating process, the viscosity of the paper coating is relatively low at high
564 shear rates. After being transferred to the paper surface, CNFs in the coating form a highly
565 viscous layer when the shear force ends [64]. Na10_1_N and Na10_2_N, due to their low
566 viscosity, may be applied as reinforcement agents, where the viscosity is not a limiting factor.

567 The viscosities of the Na10_1_N and Na10_2_N samples at a shear rate of 100 s^{-1} are
568 extremely low (8 mPa.s and 2 mPa.s, respectively), indicating that they have more free water in
569 the suspension and would not be effective as rheological modifiers in the present conditions.
570 This free water in greater quantities can harm the healing process of a cement system.

571 **3.7 Mechanical performance of the CNFs films**

572 Table 4 shows the average and standard deviation values of the mechanical properties of
573 different CNFs films.

574 **Table 4:** Average and standard deviation values of tensile strength, Young's modulus, and elongation at
575 break of the nanostructured films from CNFs under different conditions. *It was impossible to perform

576 the test on EUC10% 2H because it was not possible to form films for this treatment. Different letters in
577 the same column indicate significant ($\rho \leq 0.05$) differences between the samples for Tukey's test.

Samples	Tensile strength (MPa)	Young's modulus (GPa)	Elongation at break (%)
Untreated_N	41.5 ± 5.5^{b}	3.8 ± 0.8^{bc}	1.8 ± 0.4^{a}
TOCNF	54.5 ± 5.5^{a}	8.5 ± 0.9^{a}	1.2 ± 0.3^{b}
Na5_2_N	45.9 ± 6.5^{ab}	4.2 ± 0.5^{b}	1.7 ± 0.3^{a}
Na10_1_N	24.9 ± 6.4^{c}	3.0 ± 0.6^{c}	1.1 ± 0.2^{b}
Na10_2_N*	-	-	-

578

579 TOCNF had higher averages of tensile strength and Young's modulus, whereas
580 Na10_1_N had lower averages. Untreated_N and Na5_2_N presented intermediate averages and
581 did not differ from each other. This result can be attributed to the reduction of empty spaces in
582 the interfaces between nanofibrils, promoted by the increase in the highly individualized
583 nanofibril surface area. However, CNFs Na10_1_N (24.9 ± 6.4 MPa) exhibited lower
584 nanofibrillation efficiency. A higher free volume between fibrils may have resulted in a
585 reduction in the crystallinity index, thereby decreasing the tensile strength and Young's modulus
586 (3.0 GPa) of fibrils themselves [65].

587 Another factor that explains the decrease in the mechanical properties of the CNFs
588 Na10_1_N films is the partial conversion of cellulose I to cellulose II. In the literature, cellulose
589 II has a lower Young's modulus than cellulose I [66].

590 The hemicellulose content can also influence the mechanical properties of films, as
591 shown in the previous section. Na10_1 demonstrated a lower hemicellulose content (~4%) than
592 Untreated (~16%), TOCNF (~15%), and Na5_2 (~10%). When the hemicellulose content
593 declined drastically, the mechanical properties of the Na10_1 sample film may have decreased.
594 The superiority of samples with a higher hemicellulose content on mechanical properties may
595 be due to many hydroxyl groups that increase the hydrogen bond energy density [67].
596 Furthermore, the presence of more xylan contributes to the adhesion between CNFs in the dried
597 state, leading to an improvement in the strength of the CNFs films [68].

598 The elongation at break averages of Untreated_N and Na5_2_N were similar.
599 Na10_1_N presented a lower average, although it was similar to TOCNF. In the case of

Na10_1_N (1.1 ± 0.2%), the decrease may indicate that hemicellulose is essential for plastic deformation of CNFs films because of their amorphous nature [69].

Excessive removal of hemicellulose caused coalescence between fibrils, impeding the formation of an interconnected network resulting in low nanofibrillation (Fig. 3D). As already reported, these polymers inhibit the coalescence between microfibrils, facilitating cell wall delamination.

3.8 Effect of modifications on quality of cellulose nanofibers

The CNFs produced after the different treatments were evaluated by the simplified quality index (*Q.I.) proposed by Desmaisons et al. [21], obtaining the values shown in Table 5.

Table 5: Simplified quality indices of CNFs produced by different treatments. Different letters in the same column indicate significant ($\rho \leq 0.05$) differences between the samples for Tukey's test.

Sample	Turbidity (NTU)	Transparency (%)	Young's modulus (GPa)	Microsize area (µm²)	*Q.I.
Untreated_N	377 ± 3^{c}	29 ± 4^{c}	3.8 ± 0.8^{bc}	32.8 ± 1^{bc}	63 ± 3^{b}
TOCNF	83 ± 5^{e}	77 ± 9^{a}	8.5 ± 0.9^{a}	22.8 ± 1^{c}	80 ± 3^{a}
Na5_2_N	359 ± 4^{d}	51 ± 4^{b}	4.2 ± 0.5b	28.7 ± 7^{c}	68 ± 3^{b}
Na10_1_N	706 ± 8^{b}	46 ± 8^{b}	3.0 ± 0.6^{c}	52.5 ± 13^{b}	51 ± 3^{c}
Na10_2_N	912 ± 1^{a}	43 ± 1^{bc}	-	121.2 ± 22^{a}	32 ± 1^{d}

The TOCNF treatment obtained the highest score in the quality index. It was observed that the Na5_2_N treatment obtained a quality index score statistically equal to that of the Untreated_N sample. However, it promoted economical energy consumption during nanofibrillation, reflecting the efficiency of this treatment in reducing the recalcitrance of the fibers, facilitating its deconstruction into smaller structures. The quality index score for the Untreated_N sample was similar to those obtained by Espinosa et al. [70] (59.5 ± 5.5)), while the Na10_1_N treatment obtained a lower value than that found by Banvillet et al. [48] (54.0 ± 2.8)).

The Na10_2_N treatment resulted in the lowest score, demonstrating the influence of the reaction time of the alkaline treatment. As already discussed in previous sections, this behavior may be associated with the hemicellulose content in the samples, which facilitates the

deconstruction of the fiber cell wall, as shown in the results of the microsized area, where the treatment with less hemicellulose showed a larger area of non-nanofibrillated particles.

The NaOH treatments, in general, promoted increased transparency of the samples compared to Untreated_N, which can be attributed to the disorder caused by the alkaline treatment in the cellulose structure during the conversion from the native form to cellulose II and to the increased presence of amorphous structures [71].

4 Conclusions

NaOH treatments under different conditions promoted changes in fiber properties and the crystalline structure of cellulose. The partial removal of hemicellulose to a range close to 10% and the coexistence of cellulose I and cellulose II polymorphs (in low quantity) facilitated the production of CNFs. Hemicellulose influenced the rheological behavior of the CNFs because its removal reduced the formation of complex networks between nanofibrils because it has free hydrogen bonding sites that allow for cross-linking between cellulose chains. It also influenced their mechanical performance; the higher removal impaired the entanglement of the nanofibrils, weakening the structure of the films.

Acknowledgments

The authors thank the Research Support Foundation of Minas Gerais (FAPEMIG), the National Council for Scientific and Technological Development (CNPq), the Brazilian Federal Agency for the Support and Evaluation of Graduate Education (CAPES; Funding Code 001), and the Wood Science and Technology graduate program from Federal University of Lavras for providing equipment and financial support. We also thank the Laboratoire Génie des Procédés Papetiers (LGP2) as a part of the LabEx Tec 21 (Investissements d'Avenir–grant agreement no. ANR-11-LABX- 0030) and of the Energies du Futur and PolyNat Carnot Institutes. The Center of Microscopy at the Federal University of Minas Gerais (http://www.microscopia.ufmg.br) for providing the equipment and technical support for experiments involving TEM and Thierry Encinas from CMTC - Grenoble for the XRD analysis.

Conflict of interest

The authors declare that they have no conflicts of interest.

5 References

[1] H. Wang, D. Li, H. Yano, K. Abe, Preparation of tough cellulose II nanofibers with high thermal stability from wood, Cellulose. 21 (2014) 1505–1515. doi:10.1007/s10570-014-0222-6.

[2] S. Sharma, S.S. Nair, Z. Zhang, A.J. Ragauskas, Y. Deng, Characterization of micro fibrillation process of cellulose and mercerized cellulose pulp, RSC Adv. 5 (2015) 63111–63122. doi:10.1039/c5ra09068g.

[3] V. Kumar, B. Nazari, D. Bousfield, M. Toivakka, Rheology of microfibrillated cellulose suspensions in pressure-driven flow, Appl. Rheol. 26 (2016) 1–11. doi:10.3933/ApplRheol-26-43534.

[4] M.A. Hubbe, P. Tayeb, M. Joyce, P. Tyagi, M. Kehoe, K. Dimic-Misic, L. Pal, Rheology of nanocellulose-rich aqueous suspensions: A review, BioResources. 12 (2017) 9556–9661. doi:10.15376/biores.12.4.Hubbe.

[5] M.M. Rueda, M.C. Auscher, R. Fulchiron, T. Périé, G. Martin, P. Sonntag, P. Cassagnau, Rheology and applications of highly filled polymers: A review of current understanding, Prog. Polym. Sci. 66 (2017) 22–53. doi:10.1016/j.progpolymsci.2016.12.007.

[6] T. Moberg, K. Sahlin, K. Yao, S. Geng, G. Westman, Q. Zhou, K. Oksman, M. Rigdahl, Rheological properties of nanocellulose suspensions: effects of fibril/particle dimensions and surface characteristics, Cellulose. 24 (2017) 2499–2510. doi:10.1007/s10570-017-1283-0.

[7] O. Nechyporchuk, M.N. Belgacem, J. Bras, Production of cellulose nanofibrils: A review of recent advances, Ind. Crops Prod. 93 (2016) 2–25. doi:10.1016/j.indcrop.2016.02.016.

[8] N. V. Ehman, A.F. Lourenço, B.H. McDonagh, M.E. Vallejos, F.E. Felissia, P.J.T. Ferreira, G. Chinga-Carrasco, M.C. Area, Influence of initial chemical composition and characteristics of pulps on the production and properties of lignocellulosic nanofibers, Int. J. Biol. Macromol. 143 (2020) 453–461. doi:10.1016/j.ijbiomac.2019.10.165.

[9] Y. Zhang, N. Hao, X. Lin, S. Nie, Emerging challenges in the thermal management of cellulose nanofibril-based supercapacitors, lithium-ion batteries and solar cells: A review, Carbohydr. Polym. 234 (2020) 115888. doi:10.1016/j.carbpol.2020.115888.

[10] A. Lorenci Woiciechowski, C.J. Dalmas Neto, L. Porto de Souza Vandenberghe, D.P. de Carvalho Neto, A.C. Novak Sydney, L.A.J. Letti, S.G. Karp, L.A. Zevallos Torres, C.R. Soccol, Lignocellulosic biomass: Acid and alkaline pretreatments and their effects on biomass recalcitrance – Conventional processing and recent advances, Bioresour. Technol. 304 (2020) 122848. doi:10.1016/j.biortech.2020.122848.

[11] Y. Zhao, U. Shakeel, M. Saif Ur Rehman, H. Li, X. Xu, J. Xu, Lignin-carbohydrate complexes (LCCs) and its role in biorefinery, J. Clean. Prod. 253 (2020) 120076. doi:10.1016/j.jclepro.2020.120076.

[12] S. Kishani, F. Vilaplana, W. Xu, C. Xu, L. Wågberg, Solubility of Softwood Hemicelluloses, Biomacromolecules. 19 (2018) 1245–1255. doi:10.1021/acs.biomac.8b00088.

[13] T. Rodrigues Mota, D. Matias de Oliveira, R. Marchiosi, O. Ferrarese-Filho, W. Dantas dos Santos, Plant cell wall composition and enzymatic deconstruction, AIMS Bioeng. 5 (2018) 63–77. doi:10.3934/bioeng.2018.1.63.

[14] F. Peng, J.L. Ren, B. Peng, F. Xu, R.C. Sun, J.X. Sun, Rapid homogeneous lauroylation of wheat straw hemicelluloses under mild conditions, Carbohydr. Res. 343 (2008) 2956–2962. doi:10.1016/j.carres.2008.08.023.

[15] K. Kulasinski, L. Salme, D. Derome, J. Carmeliet, Moisture adsorption of glucomannan and xylan hemicelluloses, Cellulose. 23 (2016) 1629–1637. doi:10.1007/s10570-016-0944-8.

[16] L. Salmén, On the organization of hemicelluloses in the wood cell wall, Cellulose. 9 (2022). doi:10.1007/s10570-022-04425-9.

[17] S. Iwamoto, K. Abe, H. Yano, The effect of hemicelluloses on wood pulp nanofibrillation and nanofiber network characteristics, Biomacromolecules. 9 (2008) 1022–1026. doi:10.1021/bm701157n.

[18] M.C. Dias, M.C. Mendonça, R.A.P. Damásio, Influence of hemicellulose content of Eucalyptus and Pinus fibers on the grinding process for obtaining cellulose micro / nanofibrils, Holzforschung. 73 (2019) 1035–1046.

[19] H. Fukuzumi, T. Saito, T. Iwata, Y. Kumamoto, A. Isogai, Transparent and high gas barrier films of cellulose nanofibers prepared by TEMPO-mediated oxidation, Biomacromolecules. 10 (2009) 162–165. doi:10.1021/bm801065u.

[20] L.E. Silva, A. de A. dos Santos, L. Torres, Z. McCaffrey, A. Klamczynski, G. Glenn, A.R. de Sena Neto, D. Wood, T. Williams, W. Orts, R.A.P. Damásio, G.H.D. Tonoli, Redispersion and structural change evaluation of dried microfibrillated cellulose, Carbohydr. Polym. 252 (2021). doi:10.1016/j.carbpol.2020.117165.

[21] J. Desmaisons, E. Boutonnet, M. Rueff, A. Dufresne, J. Bras, A new quality index for benchmarking of different cellulose nanofibrils, Carbohydr. Polym. 174 (2017) 318–329. doi:10.1016/j.carbpol.2017.06.032.

[22] L.C.E. da Silva, A. Cassago, L.C. Battirola, M. do C. Gonçalves, R. V. Portugal, Specimen preparation optimization for size and morphology characterization of nanocellulose by TEM, Cellulose. 27 (2020) 5435–5444. doi:10.1007/s10570-020-03116-7.

[23] J. Schindelin, I. Arganda-Carreras, E. Frise, V. Kaynig, M. Longair, T. Pietzsch, S. Preibisch, C. Rueden, S. Saalfeld, B. Schmid, J.Y. Tinevez, D.J. White, V. Hartenstein, K. Eliceiri, P. Tomancak, A. Cardona, Fiji: An open-source platform for biological-image analysis, Nat. Methods. 9 (2012) 676–682. doi:10.1038/nmeth.2019.

[24] Y. Nishiyama, P. Langan, H. Chanzy, Crystal Structure and Hydrogen-Bonding System in Cellulose Iβ from Synchrotron X-ray and Neutron Fiber Diffraction, J. Am. Chem. Soc. 124 (2002) 9074–9082. doi:10.1021/ja0257319.

[25] A.D. French, Increment in evolution of cellulose crystallinity analysis, Cellulose. 27 (2020) 5445–5448. doi:10.1007/s10570-020-03172-z.

[26] A. El Oudiani, Y. Chaabouni, S. Msahli, F. Sakli, Crystal transition from cellulose i to cellulose II in NaOH treated Agave americana L. fibre, Carbohydr. Polym. 86 (2011) 1221–1229. doi:10.1016/j.carbpol.2011.06.037.

[27] L.O. Souza, O.A. Lessa, M.C. Dias, G.H.D. Tonoli, D.V.B. Rezende, M.A. Martins, I.C.O. Neves, J.V. de Resende, E.E.N. Carvalho, E.V. de Barros Vilas Boas, J.R. de Oliveira, M. Franco, Study of morphological properties and rheological parameters of cellulose nanofibrils of cocoa shell (Theobroma cacao L.), Carbohydr. Polym. 214 (2019). doi:10.1016/j.carbpol.2019.03.037.

[28] R. Sothornvit, S.I. Hong, D.J. An, J.W. Rhim, Effect of clay content on the physical and antimicrobial properties of whey protein isolate/organo-clay composite films, LWT - Food Sci. Technol. 43 (2010) 279–284. doi:10.1016/j.lwt.2009.08.010.

[29] P. Tao, Z. Wu, C. Xing, Q. Zhang, Z. Wei, S. Nie, Effect of enzymatic treatment on the thermal stability of cellulose nanofibrils, Cellulose. 26 (2019) 7717–7725. doi:10.1007/s10570-019-02634-3.

[30] M.C. Li, Q. Wu, K. Song, S. Lee, Y. Qing, Y. Wu, Cellulose Nanoparticles: Structure-Morphology-Rheology Relationships, ACS Sustain. Chem. Eng. 3 (2015) 821–832. doi:10.1021/acssuschemeng.5b00144.

[31] T. Pääkkönen, K. Dimic-Misic, H. Orelma, R. Pönni, T. Vuorinen, T. Maloney, Effect of xylan in hardwood pulp on the reaction rate of TEMPO-mediated oxidation and the rheology of the final nanofibrillated cellulose gel, Cellulose. 23 (2016) 277–293. doi:10.1007/s10570-015-0824-7.

[32] C.K. Saurabh, A. Mustapha, M.M. Masri, A.F. Owolabi, M.I. Syakir, R. Dungani, M.T. Paridah, M. Jawaid, H.P.S. Abdul Khalil, Isolation and characterization of cellulose nanofibers from gigantochloa scortechinii as a reinforcement material, J. Nanomater. 2016 (2016). doi:10.1155/2016/4024527.

[33] S. Ventura-Cruz, A. Tecante, Extraction and characterization of cellulose nanofibers from Rose stems (Rosa spp.), Carbohydr. Polym. 220 (2019) 53–59. doi:10.1016/j.carbpol.2019.05.053.

[34] S. Fujisawa, Y. Okita, H. Fukuzumi, T. Saito, A. Isogai, Preparation and characterization of TEMPO-oxidized cellulose nanofibril films with free carboxyl groups, Carbohydr. Polym. 84 (2011) 579–583. doi:10.1016/j.carbpol.2010.12.029.

[35] L.V. Cabañas-Romero, C. Valls, S. V. Valenzuela, M.B. Roncero, F.I.J. Pastor, P. Diaz, J. Martínez, Bacterial Cellulose-Chitosan Paper with Antimicrobial and Antioxidant Activities, Biomacromolecules. 21 (2020) 1568–1577. doi:10.1021/acs.biomac.0c00127.

[36] L.M. Ilharco, R. Brito De Barros, Aggregation of pseudoisocyanine iodide in cellulose acetate films: Structural characterization by FTIR, Langmuir. 16 (2000) 9331–9337. doi:10.1021/la000579e.

[37] J. Yuan, C. Yi, H. Jiang, F. Liu, G.J. Cheng, Direct Ink Writing of Hierarchically Porous Cellulose/Alginate Monolithic Hydrogel as a Highly Effective Adsorbent for Environmental Applications, ACS Appl. Polym. Mater. 3 (2021) 699–709. doi:10.1021/acsapm.0c01002.

[38] B. Soni, E.B. Hassan, B. Mahmoud, Chemical isolation and characterization of different cellulose nanofibers from cotton stalks, Carbohydr. Polym. 134 (2015) 581–589. doi:10.1016/j.carbpol.2015.08.031.

[39] Y. Lu, P. Tao, N. Zhang, S. Nie, Preparation and thermal stability evaluation of cellulose nanofibrils from bagasse pulp with differing hemicelluloses contents, Carbohydr. Polym. 245 (2020) 116463. doi:10.1016/j.carbpol.2020.116463.

[40] G. Tondi, A. Petutschnigg, Middle infrared (ATR FT-MIR) characterization of industrial tannin extracts, Ind. Crops Prod. 65 (2015) 422–428. doi:10.1016/j.indcrop.2014.11.005.

[41] C. Soares, F. Mário, V. Scatolino, L. Eduardo, S. Maria, A. Martins, M. Guimarães, J. Gustavo, H. Denzin, Valorization of Jute Biomass : Performance of Fiber – Cement

Composites Extruded with Hybrid Reinforcement (Fibers and Nanofibrils), Waste and Biomass Valorization. (2021). doi:10.1007/s12649-021-01394-1.

[42] H. Lee, J. Sundaram, L. Zhu, Y. Zhao, S. Mani, Improved thermal stability of cellulose nano fi brils using low-concentration alkaline pretreatment, Carbohydr. Polym. 181 (2018) 506–513. doi:10.1016/j.carbpol.2017.08.119.

[43] T.M. Tenhunen, M.S. Peresin, P.A. Penttilä, J. Pere, R. Serimaa, T. Tammelin, Significance of xylan on the stability and water interactions of cellulosic nanofibrils, React. Funct. Polym. 85 (2014) 157–166. doi:10.1016/j.reactfunctpolym.2014.08.011.

[44] E. Jin, J. Guo, F. Yang, Y. Zhu, J. Song, Y. Jin, O.J. Rojas, On the polymorphic and morphological changes of cellulose nanocrystals (CNC-I) upon mercerization and conversion to CNC-II, Carbohydr. Polym. 143 (2016) 327–335. doi:10.1016/j.carbpol.2016.01.048.

[45] G.H.D. Tonoli, K.M. Holtman, G. Glenn, A.S. Fonseca, D. Wood, T. Williams, V.A. Sa, L. Torres, A. Klamczynski, W.J. Orts, Properties of cellulose micro/nanofibers obtained from eucalyptus pulp fiber treated with anaerobic digestate and high shear mixing, Cellulose. 23 (2016) 1239–1256. doi:10.1007/s10570-016-0890-5.

[46] S. Nam, A.D. French, B.D. Condon, M. Concha, Segal crystallinity index revisited by the simulation of X-ray diffraction patterns of cotton cellulose Iβ and cellulose II, Carbohydr. Polym. 135 (2016) 1–9. doi:10.1016/j.carbpol.2015.08.035.

[47] Y. Chen, B. Geng, J. Ru, C. Tong, H. Liu, J. Chen, Correction to: Comparative characteristics of TEMPO-oxidized cellulose nanofibers and resulting nanopapers from bamboo, softwood, and hardwood pulps, Cellulose. 25 (2018) 895. doi:10.1007/s10570-017-1553-x.

[48] G. Banvillet, G. Depres, N. Belgacem, J. Bras, Alkaline treatment combined with enzymatic hydrolysis for efficient cellulose nanofibrils production, Carbohydr. Polym. 255 (2021). doi:10.1016/j.carbpol.2020.117383.

[49] A. Isogai, T. Saito, H. Fukuzumi, TEMPO-oxidized cellulose nanofibers, Nanoscale. 3 (2011) 71–85. doi:10.1039/c0nr00583e.

[50] Z. Ling, S. Chen, X. Zhang, F. Xu, Exploring crystalline-structural variations of cellulose during alkaline pretreatment for enhanced enzymatic hydrolysis, Bioresour. Technol. 224 (2017) 611–617. doi:10.1016/j.biortech.2016.10.064.

[51] A.I. Koponen, The effect of consistency on the shear rheology of aqueous suspensions of cellulose micro- and nanofibrils : a review, Cellulose. 0123456789 (2019). doi:10.1007/s10570-019-02908-w.

[52] A. Naderi, T. Lindström, T. Pettersson, The state of carboxymethylated nanofibrils after homogenization-aided dilution from concentrated suspensions: A rheological perspective, Cellulose. 21 (2014) 2357–2368. doi:10.1007/s10570-014-0329-9.

[53] F. Serra-Parareda, Q. Tarrés, P. Mutjé, A. Balea, C. Campano, J.L. Sánchez-Salvador, C. Negro, M. Delgado-Aguilar, Correlation between rheological measurements and morphological features of lignocellulosic micro/nanofibers from different softwood sources, Int. J. Biol. Macromol. 187 (2021) 789–799. doi:10.1016/j.ijbiomac.2021.07.195.

[54] E.J. Foster, R.J. Moon, U.P. Agarwal, M.J. Bortner, J. Bras, S. Camarero-Espinosa, K.J. Chan, M.J.D. Clift, E.D. Cranston, S.J. Eichhorn, D.M. Fox, W.Y. Hamad, L. Heux, B. Jean,

M. Korey, W. Nieh, K.J. Ong, M.S. Reid, S. Renneckar, R. Roberts, J.A. Shatkin, J. Simonsen, K. Stinson-Bagby, N. Wanasekara, J. Youngblood, Current characterization methods for cellulose nanomaterials, Chem. Soc. Rev. 47 (2018) 2609–2679. doi:10.1039/c6cs00895j.

[55] J. Ramasamy, M. Amanullah, Nanocellulose for oil and gas field drilling and cementing applications, J. Pet. Sci. Eng. 184 (2020). doi:10.1016/j.petrol.2019.106292.

[56] L. Geng, A. Naderi, Y. Mao, C. Zhan, P. Sharma, X. Peng, B.S. Hsiao, Rheological Properties of Jute-Based Cellulose Nanofibers under Different Ionic Conditions, Umesh A, Rajai A, Akira I Nanocelluloses Their Prep. Prop. Appl. ACS Symp. Ser. (2018) 113–132. doi:10.1021/bk-2017-1251.ch006.

[57] R.H. Marchessault, F.F. Morehead, M.J. Koch, Some Hydrodynamic Properties of Neutral As Related To Size and Shape 1, J. Colloid Sci. 344 (1961) 327–344.

[58] M. Iotti, Ø.W. Gregersen, S. Moe, M. Lenes, Rheological Studies of Microfibrillar Cellulose Water Dispersions, J. Polym. Environ. 19 (2011) 137–145. doi:10.1007/s10924-010-0248-2.

[59] F. Grüneberger, T. Künniger, T. Zimmermann, M. Arnold, Rheology of nanofibrillated cellulose/acrylate systems for coating applications, Cellulose. 21 (2014) 1313–1326. doi:10.1007/s10570-014-0248-9.

[60] K. Pakutsah, D. Aht-ong, Facile isolation of cellulose nanofibers from water hyacinth using water- based mechanical de fi brillation : Insights into morphological , physical , and rheological properties, Int. J. Biol. Macromol. 145 (2020) 64–76. doi:10.1016/j.ijbiomac.2019.12.172.

[61] D. Chaussy, C. Martin, J.C. Roux, Rheological behavior of cellulose fiber suspensions: Application to paper-making processing, Ind. Eng. Chem. Res. 50 (2011) 3524–3533. doi:10.1021/ie101591s.

[62] D. Lin, P. Lopez-sanchez, N. Selway, M.J. Gidley, Food Hydrocolloids Viscoelastic properties of pectin / cellulose composites studied by QCM-D and oscillatory shear rheology, Food Hydrocoll. 79 (2018) 13–19. doi:10.1016/j.foodhyd.2017.12.019.

[63] D.M. de Carvalho, C. Moser, M.E. Lindström, O. Sevastyanova, Impact of the chemical composition of cellulosic materials on the nanofibrillation process and nanopaper properties, Ind. Crops Prod. 127 (2019) 203–211. doi:10.1016/j.indcrop.2018.10.052.

[64] C. Liu, H. Du, L. Dong, X. Wang, Y. Zhang, G. Yu, B. Li, X. Mu, H. Peng, H. Liu, Properties of Nanocelluloses and Their Application as Rheology Modifier in Paper Coating, Ind. Eng. Chem. Res. 56 (2017) 8264–8273. doi:10.1021/acs.iecr.7b01804.

[65] S. Youssefian, J.E. Jakes, N. Rahbar, Variation of Nanostructures , Molecular Interactions , and Anisotropic Elastic Moduli of Lignocellulosic Cell Walls with Moisture, Sci. Rep. (2017) 1–10. doi:10.1038/s41598-017-02288-w.

[66] T. Nishino, K. Takano, K. Nakamae, Elastic modulus of the crystalline regions of cellulose polymorphs, J. Polym. Sci. Part B Polym. Phys. 33 (1995) 1647–1651. doi:10.1002/polb.1995.090331110.

[67] S. Youssefian, N. Rahbar, Molecular origin of strength and stiffness in bamboo fibrils, Sci. Rep. 5 (2015) 1–13. doi:10.1038/srep11116.

[68] M. He, G. Yang, J. Chen, X. Ji, Q. Wang, Production and Characterization of Cellulose

Nanofibrils from Different Chemical and Mechanical Pulps, J. Wood Chem. Technol. 38 (2018) 149–158. doi:10.1080/02773813.2017.1411368.

[69] F. Ceccon, M. Matos, C. Jordão, F. Avelino, D. Lomonaco, W. Luiz, E. Magalhães, Enhanced micro fi brillated cellulose-based fi lm by controlling the hemicellulose content and MFC rheology, 218 (2019) 307–314. doi:10.1016/j.carbpol.2019.04.089.

[70] E. Espinosa, F. Rol, J. Bras, A. Rodríguez, Use of multi-factorial analysis to determine the quality of cellulose nanofibers: effect of nanofibrillation treatment and residual lignin content, Cellulose. 3 (2020). doi:10.1007/s10570-020-03136-3.

[71] W. Wang, T. Liang, H. Bai, W. Dong, X. Liu, All cellulose composites based on cellulose diacetate and nano fi brillated cellulose prepared by alkali treatment, Carbohydr. Polym. 179 (2018) 297–304. doi:10.1016/j.carbpol.2017.09.098.

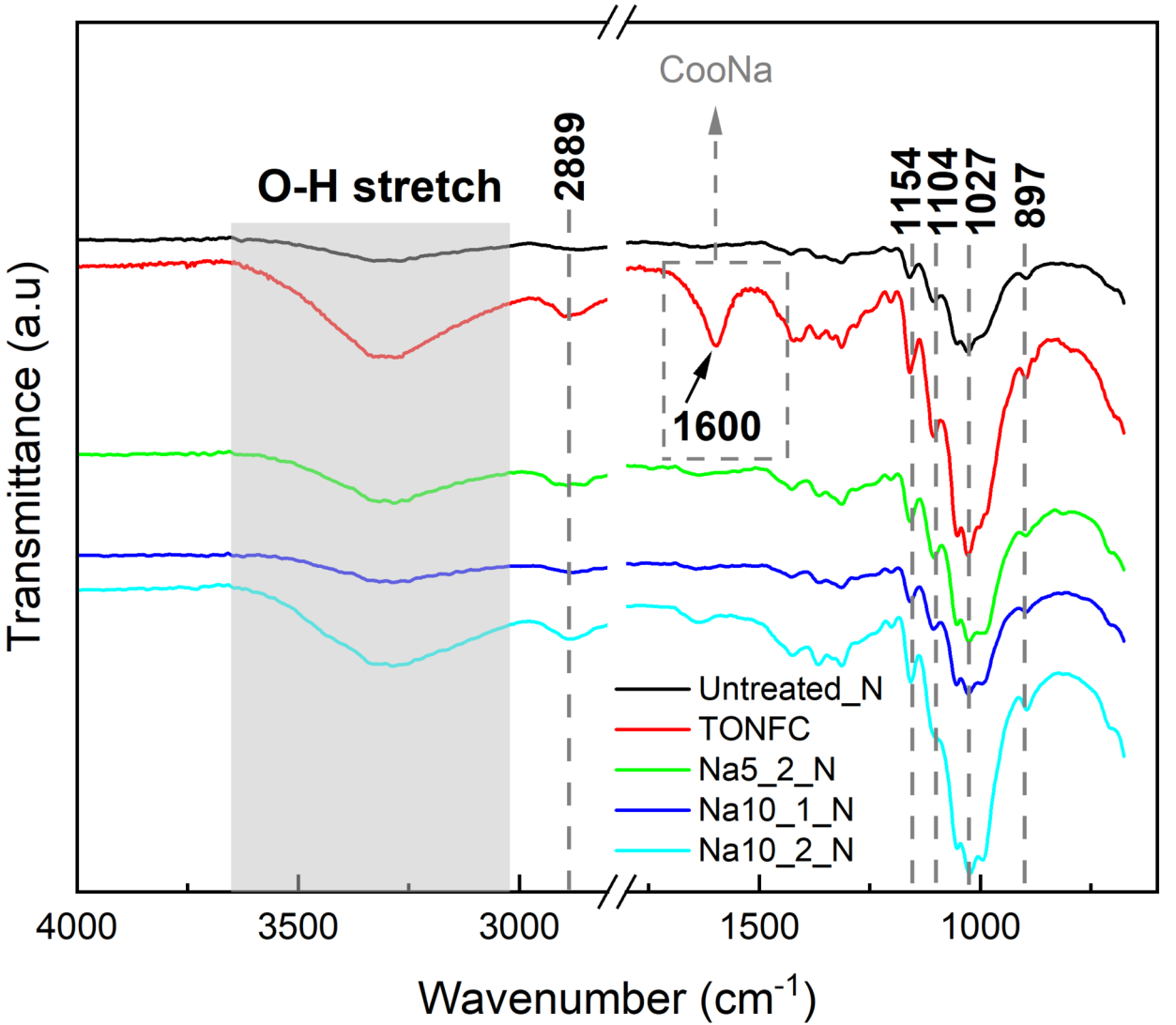
CooNa
O-H stretch
2889
1154
1104
1027
897
1600
Untreated_N
TONFC
Na5_2_N
Na10_1_N
Na10_2_N
Transmittance (a.u)
4000
3500
3000
1500
1000
Wavenumber (cm-1)

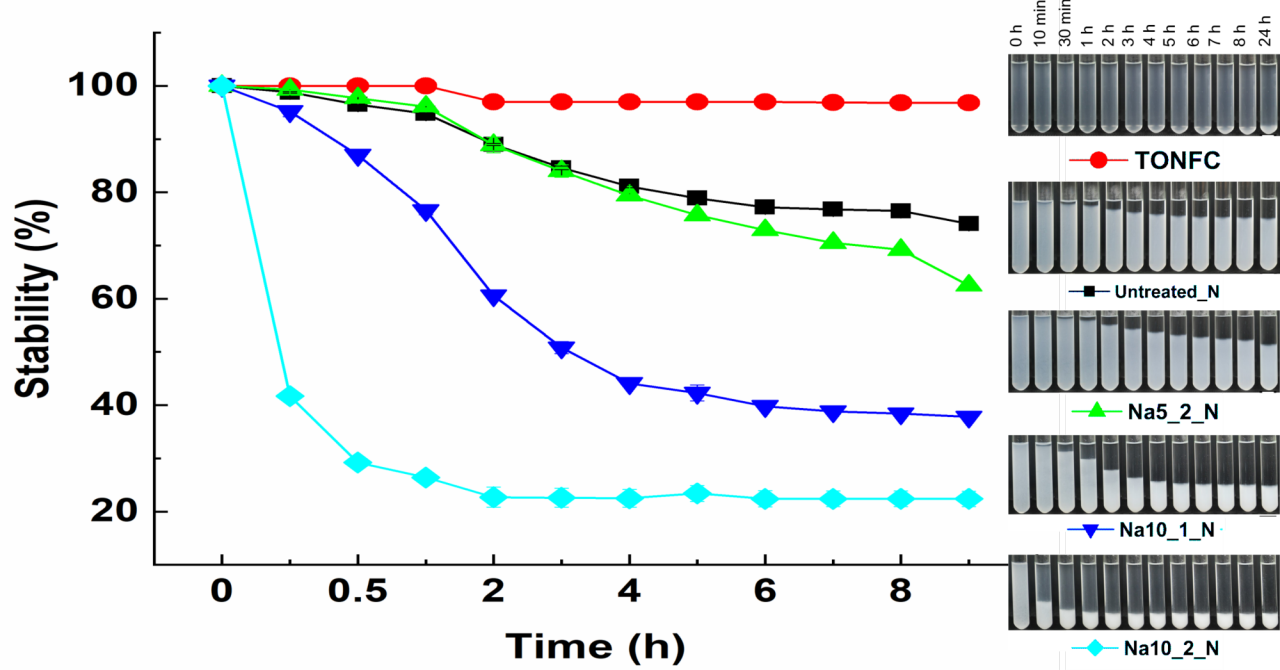
Stability (%)
100
80
60
40
20
0
0.5
2
4
6
8
Time (h)
0 h
10 min
30 min
1 h
2 h
3 h
4 h
5 h
6 h
7 h
8 h
24 h
TONFC
Untreated_N
Na5_2_N
Na10_1_N
Na10_2_N

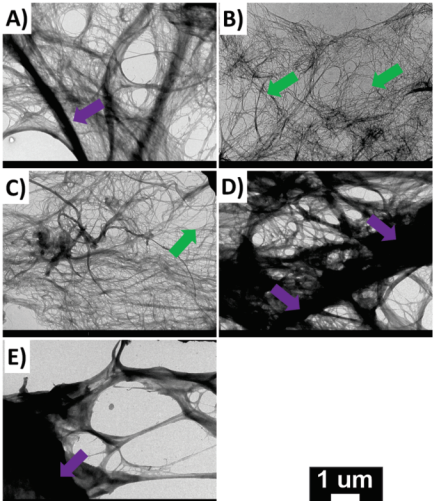
A)
B)
C)
D)
E)
1 um

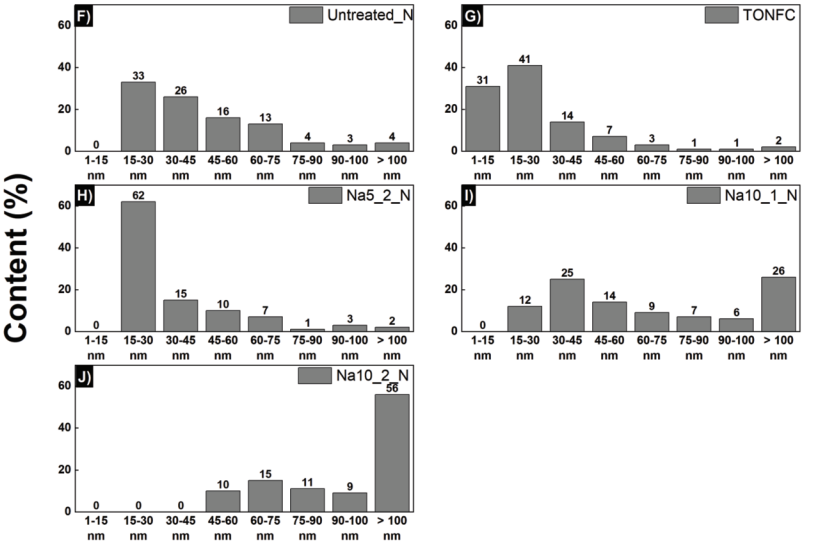
F)
Untreated_N
0
33
26
16
13
4
3
4
G)
TONFC
31
41
14
7
3
1
1
2
H)
Na5_2_N
0
62
15
10
7
1
3
2
I)
Na10_1_N
0
12
25
14
9
7
6
26
J)
Na10_2_N
0
0
0
10
15
11
9
56
1-15 nm
15-30 nm
30-45 nm
45-60 nm
60-75 nm
75-90 nm
90-100 nm
> 100 nm
Content (%)
Diameter range (nm)

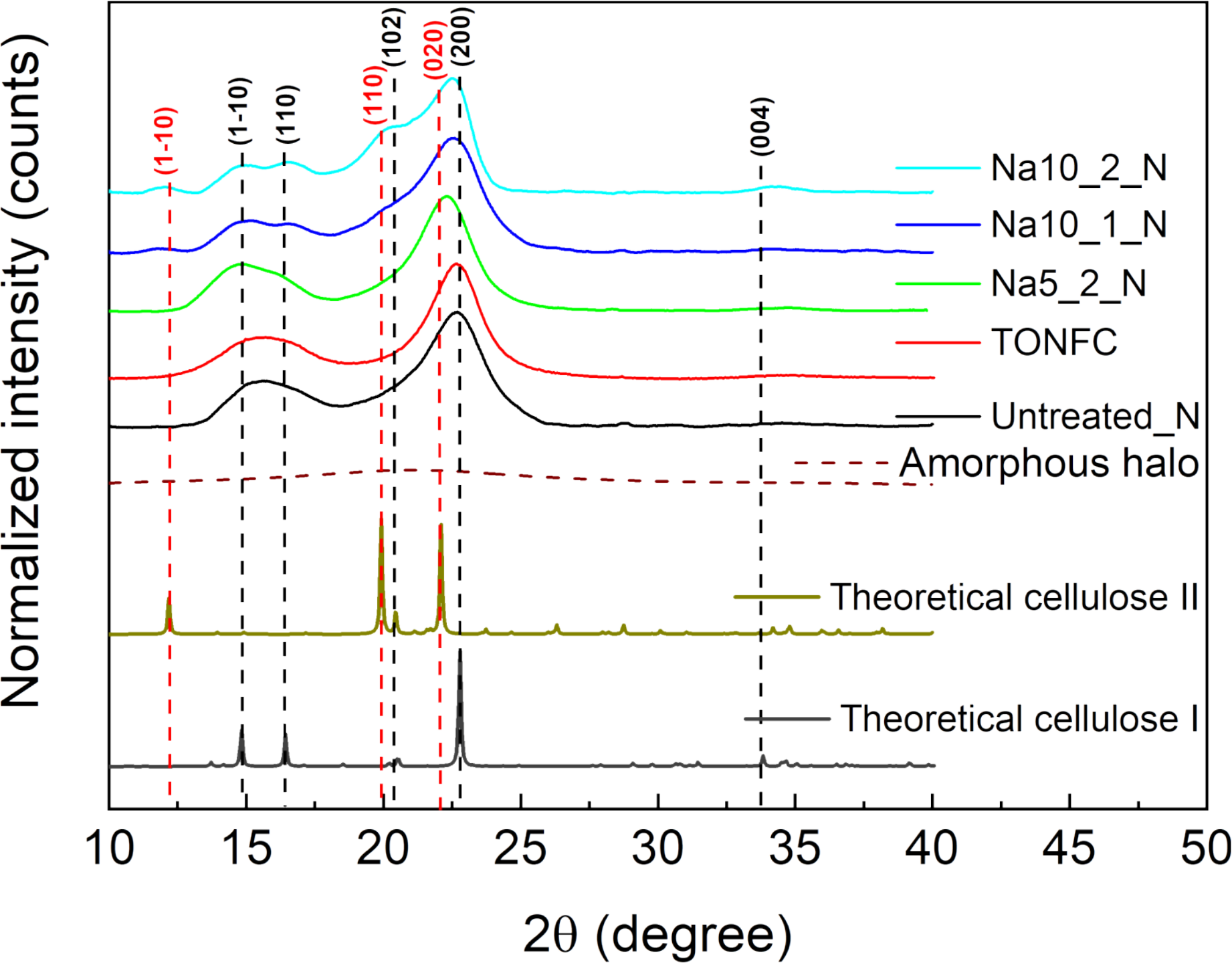

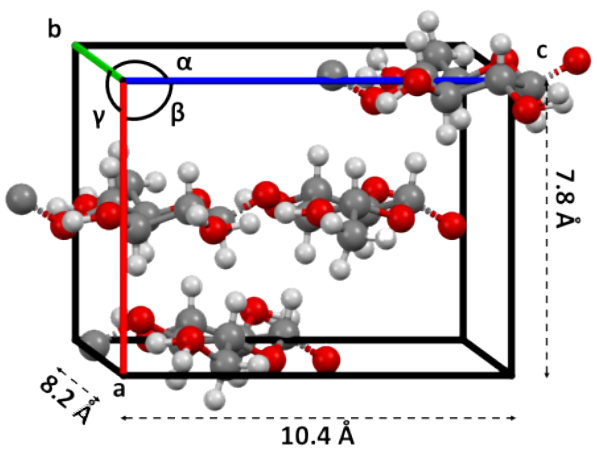

Unit cell of cellulose Iβ

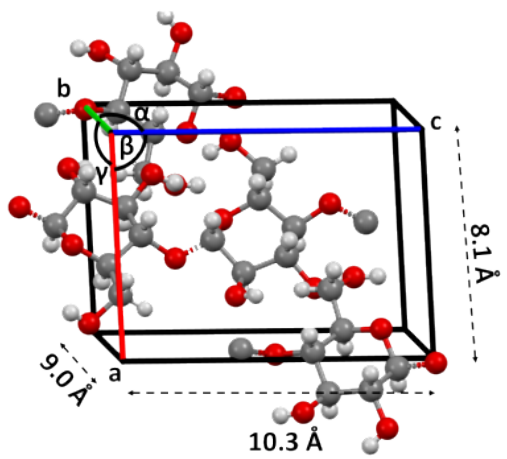

Unit cell of cellulose II

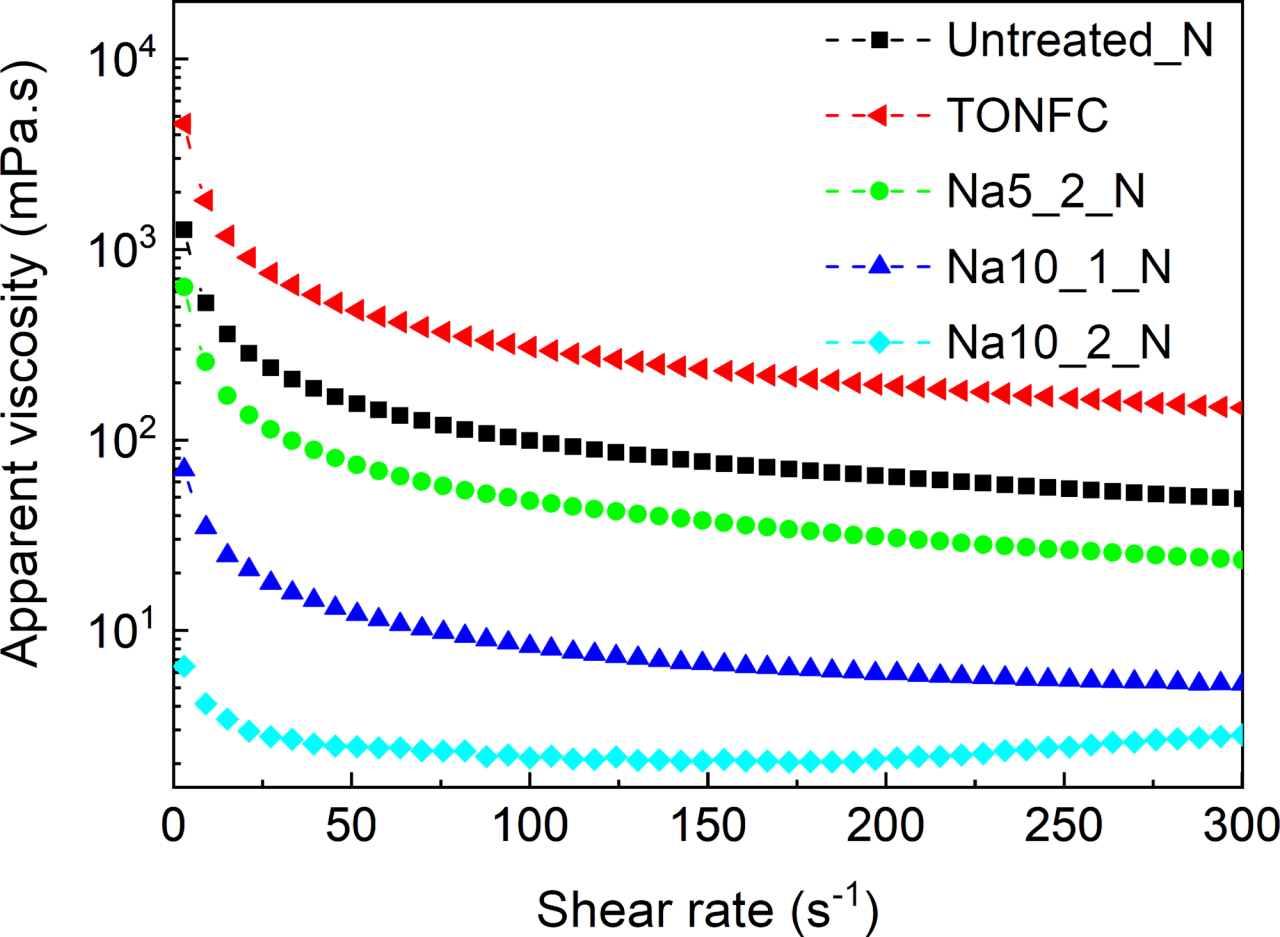
Untreated_N
TONFC
Na5_2_N
Na10_1_N
Na10_2_N
Apparent viscosity (mPa.s)
10^4
10^3
10^2
10^1
0
50
100
150
200
250
300
Shear rate (s^{-1})

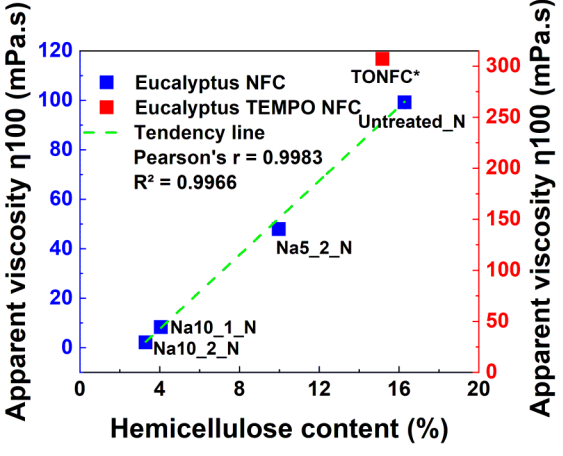
Apparent viscosity η100 (mPa.s)
Apparent viscosity η100 (mPa.s)
Hemicellulose content (%)
Eucalyptus NFC
Eucalyptus TEMPO NFC
Tendency line
Pearson's r = 0.9983
R² = 0.9966
TONFC*
Untreated_N
Na5_2_N
Na10_1_N
Na10_2_N
0
4
8
12
16
20
0
20
40
60
80
100
120
0
50
100
150
200
250
300

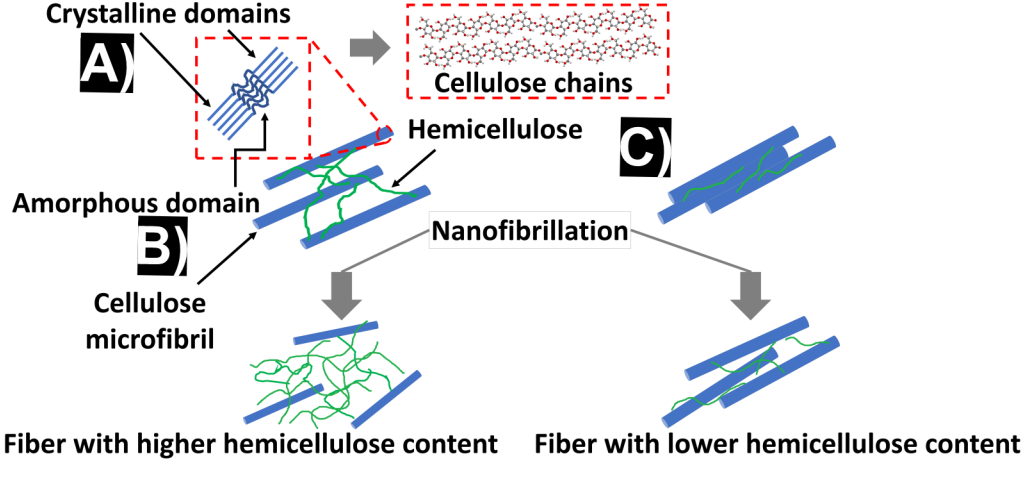
Crystalline domains
A)
Cellulose chains
Hemicellulose
C)
Amorphous domain
B)
Nanofibrillation
Cellulose
microfibril
Fiber with higher hemicellulose content
Fiber with lower hemicellulose content